Adaptive antimicrobial nanocarriers for the control of infectious biofilms

Liu, Yong

CHAPTER 3

Eradication of Multidrug-Resistant Staphylococcal Infections by Light-Activatable Micellar Nanocarriers in a Murine Model

Liu, Y., van der Mei, H. C. Zhao, B. Zhai, Y. Cheng, T. Li, Y. Zhang, Z. Busscher, H. J. Ren, Y. and Shi, L. *Adv. Funct. Mater.*, **2017**, *27*, 1701974.

ABSTRACT

Bacterial infections are mostly due to bacteria in their biofilm mode-ofgrowth, making them recalcitrant to antibiotic penetration. In addition, the number of bacterial strains intrinsically resistant to available antibiotics is alarmingly growing. This study reports that micellar nanocarriers with a poly(ethylene glycol) shell fully penetrate staphylococcal biofilms due to their biological invisibility. However, when the shell is complemented with poly(β-amino ester), these mixed-shell micelles become positively charged in the low pH environment of a biofilm, allowing not only their penetration but also their accumulation in biofilms without being washed out, as do single-shell micelles lacking the pH-adaptive feature. Accordingly, bacterial killing of multidrug resistant staphylococcal biofilms exposed to protoporphyrin IX-loaded mixed-shell micelles and after light-activation is superior compared with single-shell micelles. Subcutaneous infections in mice, induced with vancomycin-resistant, bioluminescent staphylococci can be eradicated by daily injection of photoactivatable protoporphyrin IX-loaded, mixed-shell micelles in the bloodstream and light-activation at the infected site. Micelles, which are not degraded by bacterial enzymes in the biofilm, are degraded in the liver and spleen and cleared from the body through the kidneys. Thus, adaptive micellar nanocarriers loaded with lightactivatable antimicrobials constitute a much-needed alternative to current antibiotic therapies.

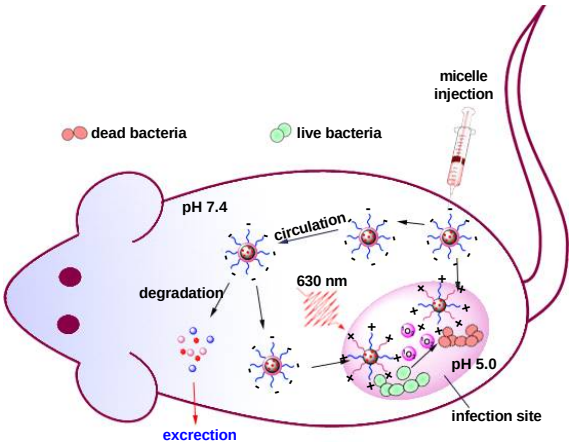

KEYWORDS: ***biofilms, infections, multidrug resistance, nanoparticles, photodynamic therapy***

INTRODUCTION

Bacterial infections are for the major part due to bacteria growing in their biofilm mode of growth.[1] In a biofilm, bacteria embed themselves in a protective matrix of self-produced extracellular polymeric substances (EPS), also known as "slime".[2–4] The EPS matrix not only protects its bacterial inhabitants against the host immune system but also against antimicrobials.[5,6] Although the recalcitrance of bacteria against antimicrobial treatment was already described by Van Leeuwenhoek in 1684,[7] long before the introduction of the word "biofilm," biofilm-associated infections still remain notoriously difficult to treat effectively. Hitherto, few antimicrobials are available that are able to penetrate the EPS matrix surrounding infectious bacteria in a biofilm-mode of growth,[8,9] while moreover the number of intrinsically antibiotic resistant strains and species is increasing at an alarming rate.[10–12]

Clinically, the problems associated with the treatment of biofilm-associated infections bear similarity with tumor treatment.[13,14] Photodynamic tumor treatment has provided a more tissue selective way with less side effects to eradicate tumors than surgery, radiotherapy, or chemotherapy.[15] In the photodynamic treatment of tumors, a nontoxic photosensitizer is light-activated to produce high local, cytotoxic concentrations of reactive oxygen species (ROS).[14,16] ROS can not only be cytotoxic but also bactericidal with no record of stimulating resistance among bacterial strains.[17,18] Accordingly, photodynamic antimicrobial chemotherapy has focused on treating planktonic bacteria and on improving ROS generation.[19–21]However, photodynamic antimicrobial chemotherapy has been little succesful with respect to bacteria in their biofilm mode of growth, due to the lack of penetration of photosensitizers into a biofilm.[22] In addition, photosensitizers often aggregate during transport in the bloodstream, which may reduce ROS generation.[23] Aggregation of photosensitizers in blood can be prevented by their micellar encapsulation.[24] Polymeric micellar nanocarriers equipped with stealth and pH-adaptive surface features have turned out to be ideal for transporting chemotherapeutics in the bloodstream for tumor treatment,[25] as well as for transport in blood of drugs alleviating Alzheimer's disease.[26] Whereas all polymeric micellar nanocarriers are pH-adaptive with respect to their charge and hydrophilicity up to a certain degree, only hydrophilic mixed shell polymeric micelles (MSPMs) composed of the copolymer poly(ethylene glycol)-*block*-poly(ε-caprolactone) (PEG-*b*-PCL) and poly (ε-caprolactone)-*block*-poly(β-amino ester) (PCL-*b*-PAE) show complete charge reversal from a negative charge under physiological pH to a positive charge when pH drops to below 6.5.[25,27] Acidity within infection sites has been unequivocally demonstrated for highly diverse strains including staphylococci, through a variety of techniques.[28] Low pH of infections sites[29] is mainly due to a combination of low oxygen tension triggering anaerobic fermentation and the production of organic acids.[30] Accordingly, once in the acidic environment inside a tumor or biofilm, the positive charge adapted by MSPMs targets the micelles toward negatively charged tissue or bacterial cell surfaces including infection sites *in vivo*, respectively.[27,31] Here we hypothesize that negatively charged MSPMs, loaded with protoporphyrin IX (PpIX) as a photosensitizer and composed of PEG and pH-adaptive PAE, will be able to circulate freely in the bloodstream and fully penetrate and accumulate in bacterial biofilms where they become positively charged under the low pH conditions in a biofilm to selectively target themselves to negatively charged bacterial cell surfaces. Once targeted to a bacterial cell surface, external light-activation will yield generation of ROS in the close vicinity of the target pathogens. We anticipate that these features of PpIX-loaded MSPMs will yield enhanced bacterial killing of bacteria in their biofilm mode of growth, as compared to single shell polymeric micelles (SSPMs) composed of only PEG-*b*-PCL.

In this paper, we aim to verify the above hypothesis and show that MSPMs loaded with PpIX can penetrate and accumulate more deeply into *in vitro* staphylococcal biofilms than SSPMs and kill bacteria in their biofilm-mode of growth upon lightactivation. Moreover, *in vivo* efficacy of light-activatable PpIX loaded MSPMs *vis-à-vis* SSPMs and vancomycin treatment will be demonstrated in a murine model against a vancomycin resistant staphylococcal infection using bio-optical imaging. This study was carried out with two strains of *Staphylococcus aureus* (*S. aureus*). *S. aureus* is involved in many soft tissue infections and infections associated

with biomaterials implants and devices.[32] Moreover, multidrug-resistant *S. aureus* strains are rapidly emerging.[33] In order to allow the use of bioluminescent imaging, one of the two strains used here was bioluminescent, while the other strain was green-fluorescent. Both strains were resistant to multiple antibiotics (see Table **S1**, Supporting Information), most notably vancomycin.

RESULTS

Physicochemical Characteristics of Single- and Mixed-Shell Micellar Nanocarriers. SSPMs were prepared by combining PEG_{5k}-*b*-PCL_{10k} in tetrahydrofuran in acetate buffer, while for the preparation of MSPMs, equal volumes of PEG_{5k}-*b*-PCL_{10k} and PCL_{10k}-*b*-PAE_{11k} in tetrahydrofuran were combined in acetate buffer. Resulting micelle suspensions were dialyzed in a dialysis bag to remove tetrahydrofuran and subsequently suspended in phosphate buffer. First, micelle diameters were measured using dynamic light scattering for unloaded and PpIX-loaded micelles. The widths of the intensity peaks in dynamic light scattering are rather narrow (Figure **S1A**, Supporting Information), yielding micelle diameters between 142 and 100 nm for SSPMs and MSPMs respectively, regardless of pH and PpIX-loading (Figure **1A**). Transmission electron micrographs of the micelles confirm a spherical morphology (Figure **S1B**, Supporting Information). As in vivo, micelles are exposed to blood at pH 7.4 before entering the acidic environment of a biofilm, micelle diameters were also measured after exposure to plasma at pH 7.4.[34,35] Plasma exposure slightly increased the hydrodynamic diameters of the micelles, indicating the formation of a protein corona around the micellar nanocarriers.[36] Zeta potentials of both types of micelles are negative at physiological pH 7.4 (Figure **1B**), while MSPMs become more negatively charged upon PpIX-loading, which has previously been attributed to a contribution of PpIX to the negative charge.[37] Importantly, only MSPMs acquire a positive zeta potential at pH 5.0. Exposure to plasma at pH 7.4 made the negative zeta potentials of the micelles slightly more negative, but the presence of a protein corona did not impede charge reversal upon pH decrease.

PpIX-Loading of Micelles and ROS Generation by Micellar Nanocarriers. For PpIX-loading, polymer solutions in tetrahydrofuran were first mixed with a PpIX solution in the dimethylformamide. PpIX-loadings of SSPMs and MSPMs were evidenced by strong UV–VIS absorption bands around 407 nm (Figure **2A**). UV–VIS absorbance of PpIX-loaded MSPMs was about twice stronger than of PpIX-loaded SSPMs, indicating higher loading efficiency. Fluorescence intensities of PpIX-loaded SSPMs and MSPMs at around 630 nm were similar due to self-quenching of PpIX in the micelles, but relatively weak compared to PpIX in an organic solvent (Figure **2B**).

ROS generation upon light-activation of PpIX-loaded micelles was evaluated using commercially available, water-soluble 9,10-anthracenediyl-bis(methylene)-dimalonic acid (ADA) as a $^1O_2$ probe. Trapping of ROS by ADA upon light-activation of PpIX-loaded MSPMs yielded a decrease in the absorption bands at 380 and 401 nm (Figure **2C**). Quantitative comparison of the relative absorbances of ADA upon light-activation of SSPMs and MSPMs showed a twofold higher decrease in ADA absorption bands for MSPMs than for SSPMs (Figure 2D), indicative of higher amounts of ROS generation. This is likely due to the higher loading efficacy of PpIX and its monomeric nature in MSPMs (Figure **2A**). Importantly, light-activation of ADA in absence of PpIX-loaded micelles did not cause any decrease in relative absorbance, whereas the presence of PpIX-loaded MSPMs in absence of light-activation also yielded stable absorbances. Neither UV–VIS absorption nor fluorescence emission spectra of PpIX in SSPMs and MSPMs nor ROS generation were affected by exposure of the micelles to 10% plasma.

Micellar Interaction with Staphylococci and Tissue Cells in Suspension. In order to microscopically examine micellar interactions with bacteria and tissue cells, micelles were loaded with fluorescent Nile red by mixing the polymer solutions in tetrahydrofuran with Nile red instead of PpIX solution. Nile red-loaded MSPMs were highly selective in their interaction with mammalian cells or staphylococci

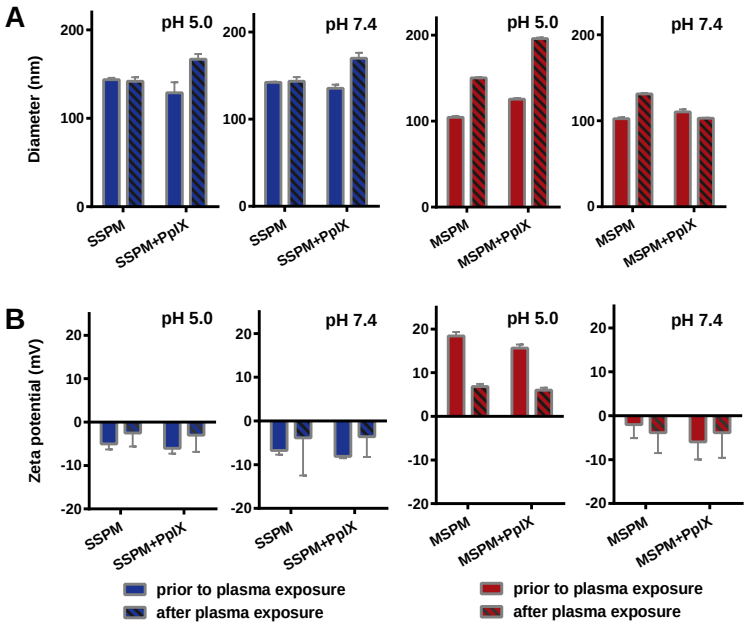

Figure 1. Micelle characterization. (**A**) Micelle diameters of SSPMs and MSPMs with or without PpIX loading measured using dynamic light scattering in 10×10^{-3} M phosphate buffer at pH 5.0 and pH 7.4 prior to and after 24 h exposure to 10% murine plasma at pH 7.4. After plasma exposure, micelles were separated from the plasma by ultracentrifugation and resuspended in 10×10^{-3} M phosphate buffer with the appropriate pH. Error bars denote the width of the intensity peaks in dynamic light scattering (see also Figure **S1**, Supporting Information). (**B**) Similar to panel (**A**), now zeta potentials. Error bars denote standard deviation (SD) values over three different experiments with separately prepared micelles.

(Figure **3A**). At neither pH did Nile red loaded MSPMs adhere to any of the three mammalian cell lines included, nor was the metabolic activity of the cells affected by growth in the presence of PpIX-loaded micelles (Figure **S2A**, Supporting Information). However, whereas Nile red-loaded micelles could not be demonstrated on staphylococcal cell surfaces at pH 7.4, Nile red-loaded MSPMs were found in ample numbers on bacterial cell surfaces at pH 5.0 (yielding yellowish fluorescence) due to the positive charge adapted by MSPMs yielding electrostatic attraction to the negatively charged staphylococcal surfaces (see Table **S2**, Supporting Information). Aliquots of light-activated staphylococcal suspensions on agar plates showed clear colony forming units in absence of PpIX loaded micelles or when exposed to light-activated PpIX-loaded SSPMs, but not when exposed to light-activated PpIX-loaded MSPMs micelles (Figure **3B**). Note that light-activation of a bacterial suspension in absence of PpIX-loaded micelles up to 60 min did not affect bacterial viability. More quantitative analysis of the reduction in the number of colony forming units (CFUs) in suspensions with PpIX-loaded micelles and staphylococci showed that the percentage viability decreased faster upon light-activation with increasing micelle concentration and to a lower level for MSPMs than for SSPMs (Figure **3C**), likely because MSPMs target better to negatively charged staphylococcal cell surfaces. Figure **3D,E** shows that 10 min light-activation suffices to achieve maximal killing of planktonic staphylococci. Light-activation of PpIX-loaded micelles during mammalian cell growth did not affect the metabolic activity of human umbilical vein endothelial cells (HUVEC) or human epithelial colorectal adenocarcinoma (Caco-2) cells, while

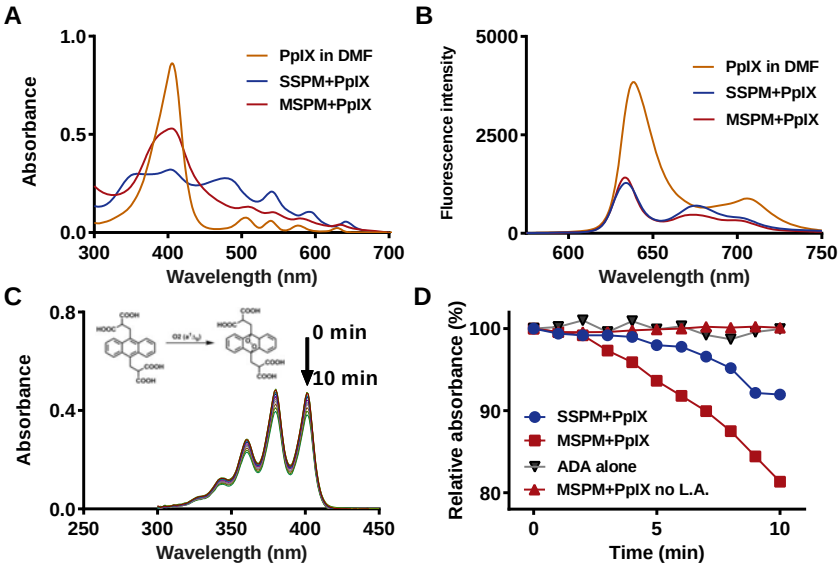

Figure 2. PpIX-loading of micelles and ROS generation. (**A**) UV–VIS absorption spectra of PpIX in SSPMs and MSPMs, measured in N,N-dimethylformamide, as well as in 10×10^{-3} M phosphate buffer (pH 7.4). (**B**) Same as panel (**A**), now fluorescence emission spectra. (**C**) UV–VIS absorption spectra of ADA and PpIX-loaded MSPMs after light-activation up to 10 min. The inset indicates conversion of ADA after reaction with ROS. (**D**) Relative UV–VIS absorption of ADA at 380 nm as a function of the light-activation time of PpIX-loaded SSPMs and MSPMs, measured in 10×10^{-3} M phosphate buffer (pH 7.4). L. A. is light-activation. Data in absence of light-activation and for light-activated ADA in absence of PpIX-loaded micelles are included as controls. Absorbance prior to light-activation was set at 100% and relative absorbances at 401 nm fully coincided with the ones measured at 380 nm.

metabolic activity of human skin fibroblasts (HSF) was only slightly reduced above micelle concentrations of 80 μg mL^{-1} (Figure **S2B**, Supporting Information). Next bio-optical imaging was applied as a rapid method to determine the effect of concentration and time on the viability, or strictly speaking, on the metabolic activity of planktonic staphylococci as a function of the light-activation time of PpIX-loaded micelles for different micelle concentrations. Bioluminescent images (Figure **3F,G**) of planktonic *S. aureus* Xen36 were quantitated using image analysis software, yielding the conclusion that MSPMs killed planktonic *S. aureus* Xen36 faster and at lower micelle concentrations than did SSPMs (**Figure 3H,I**). The percentage reduction observed upon light-activation of a suspension of bioluminescent *S. aureus* Xen36 and PpIX-loaded micelles (Figure **3H,I**) parallels the percentage reduction in staphylococcal viability (Figure **3D,E**), except for the micelle concentrations below 20 μg mL^{-1} at short light-activation times. This is due to the stimulating effect of low dose lightirradiation on bacterial metabolism,[38] similar as low doses of antibiotics increase bacterial metabolism and therewith bioluminescence.[39] For higher micelle concentration and longer light-activation times, ROS generation is sufficiently high to kill the staphylococci immediately without initial stimulation of their metabolic activity and bioluminescence.

Penetration and Accumulation in Staphylococcal Biofilms and Killing Efficacies by PpIX-Loaded Micelles. Biofilms were exposed to Nile red-loaded micelles and penetration and accumulation examined using confocal laser scanning microscopy (CLSM). The 3D CLSM images in Figure **4A** show

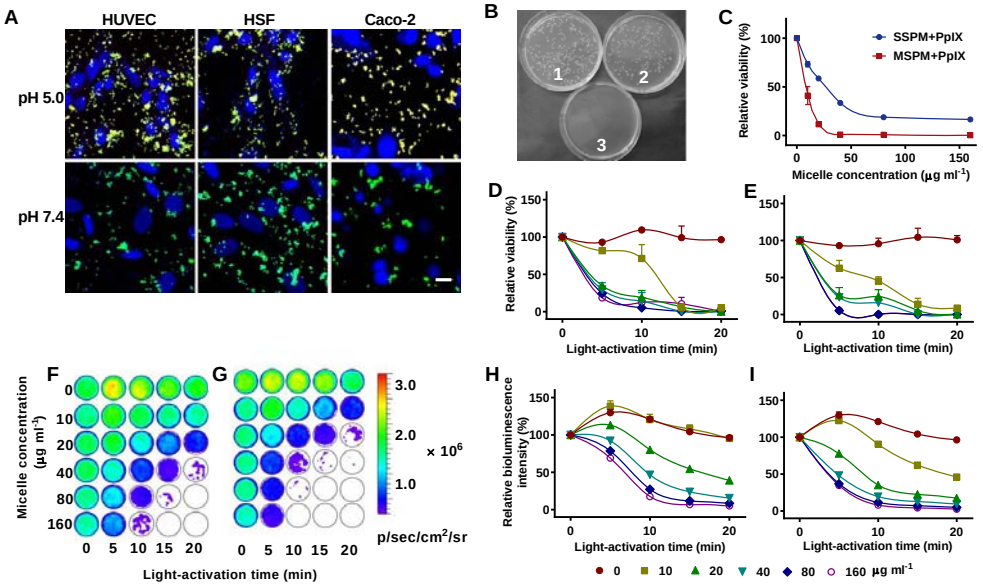

Figure 3. Selective micellar interaction with staphylococci over tissue cells in suspension and killing of planktonic bacteria. (**A**) Confocal laser scanning microscopy (CLSM) micrographs of HUVEC, HSF, and Caco-2 cells, and *S. aureus* WH^{GFP} after interaction with Nile red-loaded MSPMs in 10×10^{-3} M phosphate buffer at pH 5.0 and 7.4. Red and blue fluorescence indicate micelles and cell nuclei, while bacteria appear green, respectively. Red fluorescent micelles interacting with green fluorescent bacteria appear yellowish (at pH 5.0). Bar marker is 25 μm. (**B**) *S. aureus* Xen36 colonies on tryptic soy broth (TSB) agar plates from aliquots of staphylococcal suspensions (10^6 bacteria mL^{-1}) in phosphate buffered saline (PBS, pH 7.4) combined with PpIX-loaded SSPMs and MSPMs (40 μg mL^{-1}) and light-activated for 15 min. 1. No micelles, 2. PpIX-loaded SSPMs, and 3. PpIX-loaded MSPMs. (**C**) Relative bacterial viability of planktonic *S. aureus* Xen36 after 15 min light-activation as a function of the concentration of PpIX-loaded micelles in PBS (pH 7.4). For details, see caption of panel (**B**). Bacterial viability in PBS without micelles was set at 100%. All data are expressed as means ± SD over triplicate experiments with separately prepared micelles and different staphylococcal cultures. (**D, E**) Relative bacterial viability of planktonic *S. aureus* WH^{GFP} (10^8 bacteria mL^{-1}) in PBS (pH 7.4) as a function of the light-activation time for different concentrations of PpIX-loaded SSPMs (panel (**D**)) and MSPMs (panel (**E**)). Bacterial viability in PBS (micelle concentration 0 μg mL^{-1}) was set at 100%. All data are expressed as means ± SD values over triplicate experiments with separately prepared micelles and different staphylococcal cultures. (**F, G**) Bioluminescence images of planktonic *S. aureus* Xen36 (10^{10} bacteria mL^{-1}) in PBS after different light-activation times for different concentrations of PpIX-loaded SSPMs (panel (**F**)) and MSPMs (panel (**G**)). For details, see caption of panel (**B**). Image columns were put together from different experiments, while pseudocolor scales in different experiments were adjusted to equal scales. (**H, I**) Relative bioluminescence intensity of planktonic *S. aureus* Xen36 after different light-activation times for different concentrations of PpIX-loaded SSPMs (panel (**H**)) and MSPMs (panel (**I**)). For details, see caption to panel (**B**). Bioluminescence intensity before light-activation was set at 100%. All data are expressed as means ± SD values over triplicate experiments with separately prepared micelles and different staphylococcal cultures.

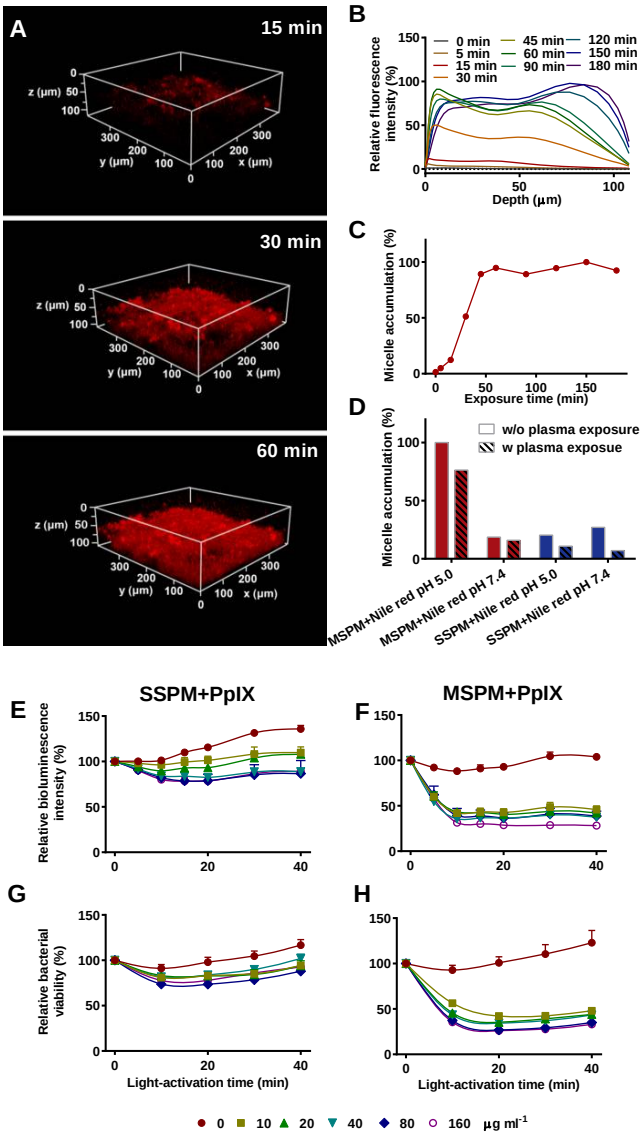

Figure 4. Penetration and accumulation of Nile-red-loaded SSPMs and MSPMs into staphylococcal biofilms and killing efficacies by PpIX-loaded micelles. (**A**) Examples of 3D CLSM micrographs of *S. aureus* WH^{GFP} biofilms after penetration and accumulation for different time intervals of Nile red-loaded MSPMs (0.1 mg mL^{-1}) in 10 × 10^{-3} M phosphate buffer at pH 5.0. (**B**) Percentage fluorescence intensity upon penetration and accumulation of Nile-red-loaded MSPMs into *S. aureus* WH^{GFP} biofilms at pH 5.0 as a function of depth in the biofilm after different time intervals up to 180 min. Percentage fluorescent intensity was expressed as the number of red-fluorescent pixels versus the total number of pixels in an image plane at a given depth. (**C**) Accumulation of Nile red-loaded MSPMs into *S. aureus* WH^{GFP} biofilms at pH 5.0 as a function of exposure time. Accumulation was expressed as the area under the curves in panel (**B**). (**D**) Accumulation of Nile-red-loaded micelles into *S. aureus* WH^{GFP} biofilms at pH 5.0 and pH 7.4, for SSPMs and MSPMs prior to and after 24 h exposure to 10% murine plasma. Accumulation was expressed as the area under curves, as presented in panel (**B**). All data are expressed as means ± SD values over triplicate experiments with separately prepared micelles and different staphylococcal cultures. (**E,F**) Relative bioluminescence intensity of *S. aureus* Xen36 in a biofilm-mode of growth after different light-activation times for different concentrations of PpIX-loaded SSPMs (panel (**E**)) and MSPMs (panel (**F**)). Bioluminescence intensity before light-activation was set at 100%. All data are expressed as means ± SD values over triplicate experiments with separately prepared micelles and different staphylococcal cultures. (**G,H**) Same as panels (**E**) and (**F**), now for the relative viability of *S. aureus* WH^{GFP} in its biofilm-mode of growth. Bacterial viability was determined by agar-plating of bacteria dispersed from the biofilms by sonication, setting bacterial viability before light-activation was set at 100%.

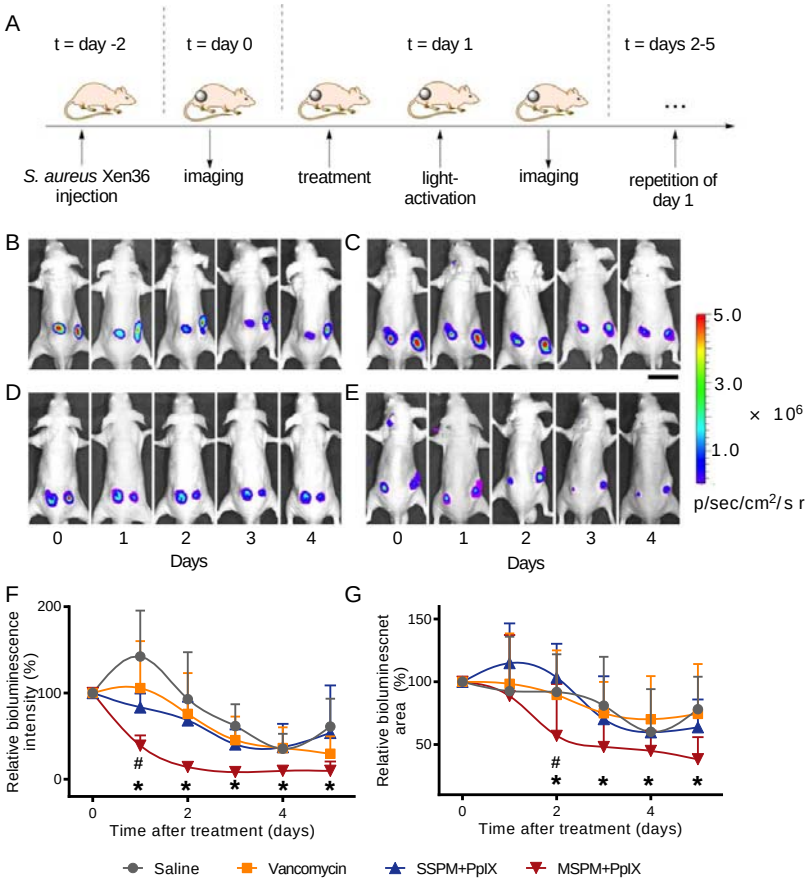

Figure 5. Micelle treatment of a subcutaneous, vancomycin-resistant staphylococcal infection in a murine model studied using bio-optical imaging. (**A**) Workflow for staphylococcal injection, treatment, and bio-optical imaging in a murine, subcutaneous infection model till sacrifice. (**B**) Time series of bioluminescence images for one and the same mouse after initiating treatment with saline (100 μL of 154 × 10^{-3} M NaCl, every 24 h). Day 0 is the day at which bioluminescence has reached a maximum in absence of treatment (see Figure **S5**, Supporting Information). Scale bar equals 2 cm. (**C**) Time series of bioluminescence in one and the same mouse after initiating treatment with vancomycin (120 mg kg^{-1}, every 24 h). Day 0 is the day at which bioluminescence has reached a maximum in absence of treatment (see Figure **S5**, Supporting Information). Scale bar equals 2 cm. (**D**) Time series of bioluminescence in one and the same mouse after initiating treatment with PpIX-loaded SSPMs (5 mg mL^{-1}, 100 μL every 24 h followed by 30 min light-activation at the infected site). Day 0 is the day at which bioluminescence has reached a maximum in absence of treatment (see Figure S5, Supporting Information). Scale bar equals 2 cm. (**E**) Same as panel (**C**), now for PpIX-loaded MSPMs. (**F**) Relative bioluminescence intensity arising from the infection site as a function of time after initiating treatment with saline, vancomycin, SSPMs, or MSPMs. Bioluminescence intensity before treatment was set at 100%. Error bars represent SD values over six mice per group. * indicates $p < 0.05$ different from all other treatments. #$p < 0.05$ different from all previous time points and the same as all following

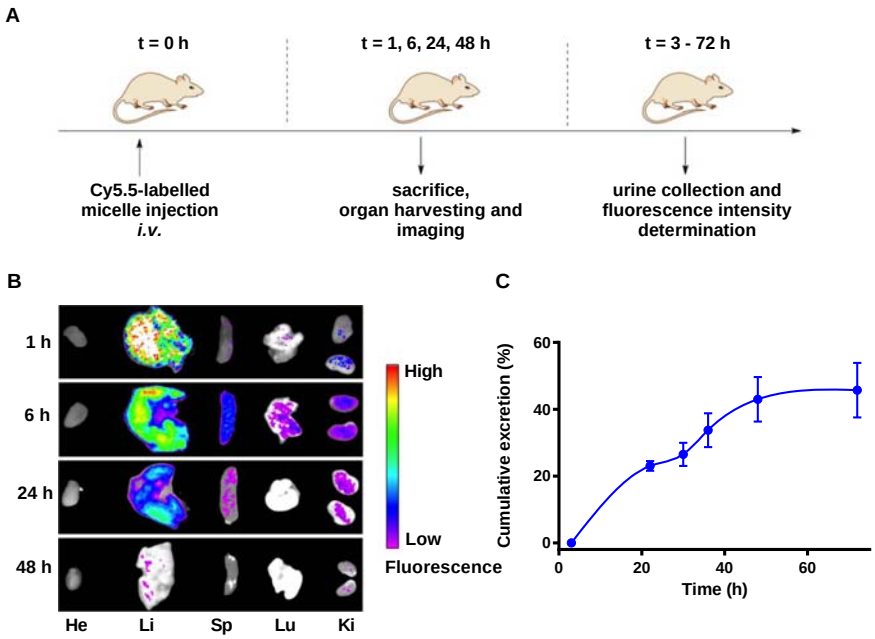

Figure 6. Clearance of micelles from the bloodstream in mice. (**A**) Workflow for micelle injection, urine collection and fluorescence imaging of micelle accumulation in different organs. Fluorescent MSPMs were injected intravenously (5 mg mL^{-1}, 200 μL) at t = 0 h. (**B**) Fluorescence images of different organs for examination of the presence of Cy5.5-loaded MSPMs in the heart (He), liver (Li), spleen (Sp), lungs (Lu), and kidneys (Ki) of mice sacrificed at different times following a single injection at t = 0 h. (**C**) Cumulative excretion of fluorescent MSPMs in urine as a function of time after injection. Excretion was expressed as a percentage with respect to the total fluorescence of the Cy5.5-loaded micelles injected. Error bars represent SD values over three mice per group.

accumulation of Nile red-loaded MSPMs into *S. aureus* WH^{GFP} biofilms. Micelles penetrate and diffuse over the depth of the biofilm progressively with exposure time (Figure **4B,C**). MSPMs accumulate in staphylococcal biofilms only at pH 5.0 and regardless of whether exposed to plasma or not. MSPMs at pH 7.4 do not penetrate and accumulate staphylococcal biofilms, while SSPMs neither accumulate in staphylococcal biofilms at pH 5.0 nor pH 7.4 (Figure **4D**). In line with the absence of penetration and accumulation of SSPMs in staphylococcal biofilms, exposure of staphylococcal biofilms to PpIX-loaded SSPM and light-activation neither yielded a reduction in biofilm bioluminescence (Figure **4E**) nor in biofilm viability (Figure **4G**). PpIX loaded MSPMs on the other hand greatly reduced staphylococcal biofilm bioluminescence (Figure **4F**) and viability (Figure **4H**), already at a micelle concentration of only 10 μg mL^{-1}.

Eradication of a Vancomycin-Resistant Staphylococcal Infection in a Murine Model. Eradication of a vancomycin-resistant staphylococcal infection was subsequently studied in a murine model

time points for PpIX-loaded MSPMs. (**G**) Same as panel (**F**), now for the relative area of the bioluminescent site. Bioluminescent area before treatment was set at 100%. * indicates $p < 0.05$ different from all other treatments. #$p < 0.05$ different from all previous time points and the same as all following time points for PpIX-loaded MSPMs.

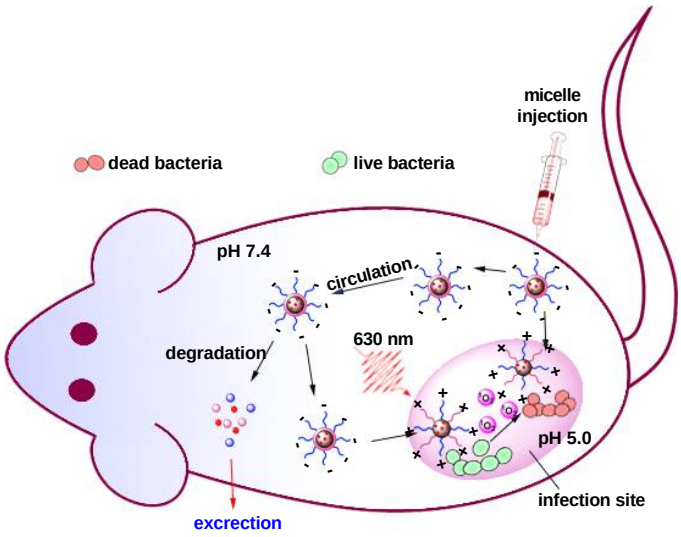

Figure 7. Schematics of the mechanisms involved in eradication of biofilmassociated infection using light-activatable PpIX-loaded MSPMs *in vivo*.

using bio-optical imaging. Dosage of infecting bacteria is critical in animal studies to cause infection and at the same time prevent death of the animals. After pilot experiments and analysis of the literature,[40,41] it was decided to inject a dose of 2×10^7 bioluminescent *S. aureus* Xen36 in the left and right flanks of the mice to initiate infection at two sites, according to the workflow in Figure **5A** (see Table **S1** of the Supporting Information for vancomycin resistance of *S. aureus* Xen36). In absence of treatment, bioluminescence reached a maximum at day 2 after injection, after which bioluminescence gradually decreased, concurrent with a decrease of the bioluminescent area. Accordingly, experiments comparing treatment with saline as a control, vancomycin and PpIX-loaded SSPMs and MSPMs were initiated at day 0, i.e., two days after injection of staphylococci. Time series of bioluminescence images for one and the same mouse after initiating the various treatments are shown in Figure **5B–E**, while quantitative analysis of the bioluminescence arising from the infected sites and the area of the infected site are presented in Figure **5F,G**. Differences in efficacies of saline, vancomycin, or SSPM treatments were small, while treatment with MSPMs induced clearance of the infection significantly sooner and to lower levels than any other treatment, including vancomycin treatment.

Clearance of Micelles from the Bloodstream in Mice. Importantly, MSPMs collected either in the biofilm (Figure **5**) or in the liver and spleen of the mice, as evidenced in a separate experiment involving mice that were injected with Cy5.5-labled fluorescent MSPMs, according to the workflow in Figure **6A**. Fluorescence of the liver and spleen was maximal 1–6 h after micelle injection (Figure **6B**), but decreased to low levels within 48 h. During these 48 h, urine was found to become fluorescent (Figure **6B,C**), indicating enzymatic breakdown of the micelles in the liver and spleen and excretion through the kidneys into the urine. After 48 h, cumulative excretion leveled off, leaving 50–60% of the fluorescence unaccounted for, probably because of enzymatic degradation of the fluorescent probe in the liver.[42]

DISCUSSION

We have developed light-activatable micellar nanocarriers multidrug-resistant staphylococcal infections in a murine model, as schematically summarized in Figure **7**. Our MSPMs are equipped with a shell composed of poly (ethylene glycol) that makes the micelles biologically invisible at physiological pH and allows them to circulate long term in the blood stream without interaction with proteins or cells. Once penetrated in a bacterial biofilm, posing a much more acidic environment to the micelles, MSPMs expose the poly (β-amino

ester) in their shell to create a positively charged micellar outer surface that interacts strongly with negatively charged bacterial cell surfaces to prevent wash-out and allow their accumulation. Taken together, these unique features allow our MSPMs to break the biofilm barrier impeding antimicrobial penetration into biofilms and, upon light-activation of their PpIX content, kills multidrug resistant staphylococci over the depth of a biofilm.

The protoporphyrinIX-loaded MSPMs composed of PEG and pH-responsive PAE are negatively charged while circulating in blood (pH 7.4) and do not interact with tissue cells. MSPMs due to their PEG shell can stealthily enter the low pH infection site where they become positively charged and bind to negatively charged bacteria. Light-activation will stimulate ROS generation and kill bacteria in their biofilm-mode of growth. Micelles that have not been degraded in the biofilm through bacterial enzymes are degraded in the liver and excreted through the kidneys.

The central point of our work is that a subcutaneous infection with vancomycin-resistant staphylococci in a murine model was cured significantly faster using light-activatable PpIX loaded MSPMs than with similarly loaded SSPMs or systemic vancomycin treatment (note that in animal models, infections are mostly cured by the immune system and dose-depending, seldom leading to death, as most human infections do).[43] Bacterial resistance to ROS generated by light-activation of PpIX has not been reported,[44] while last but not least micelles which are not degraded by the enzymes in the biofilm were degraded in the liver and spleen to find their way out of the body through excretion by the kidneys, attesting to their biological invisibility when under physiological pH conditions.

It is somewhat surprising that light-activated ROS production yields such rapid eradication of a multidrug resistant biofilm-associated infection, since ROS is extremely short-lived. On average, singlet oxygen and hydroxyl radicals have short lifetimes of only several microseconds.[45] Likely, the targeting of our pH adaptive micelles directly to the bacterial cell surface is responsible for this strong antibacterial efficacy despite ROS being short-lived. Alternative loading of the micellar nanocarriers with more stable, light-activatable antibiotics[46,47] might prolong the duration of antimicrobial activity in a biofilm after light-activation and therewith the bacterial killing efficacy. However unlike ROS, antibiotics always bear the risk of being or being ineffective due to bacterial resistance.

Photodynamic antimicrobial chemotherapy with PpIX-loaded MSPMs to treat subcutaneous infection has never been evaluated before in an animal model. Photodynamic antimicrobial chemotherapy with photosensitizers alone, without encapsulation in micelles, has been applied against oral biofilms, skin infections of surgical and burn wounds (see for an overview[48]). These applications however, do not require the targeting feature that makes our MSPMs unique. Our MSPMs can find their way through the blood circulation into an infectious biofilm remote from the injection site. Therewith also total internal, biofilm-associated infections like diabetic mice,[49] diabetic foot ulcers,[50] cystitis, prostatitis, and biofilm-associated infections of biomaterials implants and devices are within target reach by our micelles, when used in combination with advanced, deep-penetrating light-activation methods, such as laser and narrow-band LED sources with or without the use of fiber technology.[51]

The translational pathway for photodynamic antimicrobial treatment using drug-loaded micelles has been partly paved in cancer treatment. The Food and Drug Administration (FDA) has approved small molecular photosensitizers for cancer photodynamic therapy,[52,53] as well as PEG-*b*-PCL nanocarriers,[54] although not their combination.[55] MSPMs that include PAE, even though biodegradable, have not yet been FDA approved.[56] Many animal and human clinical studies have been performed pointing out advantages of photodynamic therapy toward treatment of cancer.[53] In cancer treatment, photodynamic therapy has been used in conjunction with surgery, radiotherapy, or chemotherapy. Because it is activated locally and has limited tissue penetration, photodynamic therapy can be tissue sparing[57] and lacks traditional adverse effects of radiotherapy or chemotherapy. As a drawback, intravenously administered photosensitizers may induce

skin photosensitivity, necessitating patients to avoid light,[57] typical side-effects being pain, fever, and nausea.[53] Solutions to relieve patients side-effects might be provided by the high targeting ability of our MSPMs (note that no negative side-effects of micelle injection were observed in mice, while micelles were cleared rapidly from the body). Furthermore photoswitches based on Förster resonance energy[52] transfer are currently under development that will impede inadverted light activation of photosensitizers in patients.

Benefit demonstration as part of the FDA regulatory requirements of light-activatable PpIX-loaded MSPMs to warrant further downward clinical translation toward biofilm-associated infection in general and infections caused by multidrugresistant bacteria in specific will be relatively easy considering the numbers of patients suffering from diverse types of biofilm-associated infections, including notoriously hard to treat biomaterial-associated ones.[58] Downward clinical translation of anti-infection strategies for biomaterial-associated infections such as coatings require benefit demonstration for regulatory approval in unrealistically large patients groups.[59] Therefore clinical translation of antimicrobial coatings for biomaterial implants and devices has virtually arrested nowadays.[60,61] Since further downward translation of our light-activatable PpIX-loaded MSPMs for the control of biofilm-associated infection can be done using any type of biofilm-associated infection, efficacy demonstration in clinical studies becomes statistically and therewith financially feasible, to the benefit of patients suffering from infections in general and biomaterial-associated ones at the same time.

MATERIALS AND METHODS

Preparation and Characterization of PpIX-Loaded Single-Shell and Mixed-Shell Polymeric Micelles. Micelles were prepared, as previously published.[27] For the preparation of SSPMs, PEG_{5k}-*b*-PCL_{10k} (2 mL, 5 mg mL^{-1}) in tetrahydrofuran was added dropwise into an acetate buffer (7 mL, pH 4.5, 100×10^{-3} M) at a rate of 1 droplet (20 μL) per 20 s under magnetic stirring for 4 h to form a micelle suspension. The micelle suspension was dialyzed in a dialysis bag with molecular weight cut off of 6–8 kDa against ultrapure water for 24 h to remove tetrahydrofuran. The dialyzed micelle suspension was diluted to a final concentration of 1 mg mL^{-1} and stored in a refrigerator at 4 °C. For the preparation of MSPMs, equal volumes (1 mL) of polymer (PEG_{5k}-*b*-PCL_{10k} and PCL_{10k}-*b*-PAE_{11k}, 5 mg mL^{-1}) in tetrahydrofuran were combined, as described above for SSPMs preparation. For PpIX-loading, polymer solutions in tetrahydrofuran were first mixed with a PpIX solution in the dimethylformamide (1 mg mL^{-1}). The mass ratio of PpIX to the polymers was kept at 4 wt%. The mixed polymer/PpIX solution was then added dropwise to acetate buffer (pH 4.5, 100×10^{-3}M) and followed by dialysis to remove tetrahydrofuran and dimethylformamide.

In occasional experiments, micelles were loaded with fluorescent Nile red in order to demonstrate micelle penetration and accumulation in biofilms and possible accumulation in different organs in animal experiments aimed to demonstrate in vivo efficacy of our PpIX loaded micelles. Loading the micelles with Nile red was essentially done as described above for PpIX. A Nile red stock solution in dimethylformamide (1 mg mL^{-1}, 1 wt % with respect to the amount of polymer) was mixed with polymer solution in dimethylformamide (5 mg mL^{-1}) to a total volume of 2 mL. Under rigorous magnetic stirring, acetate buffer (pH 4.5, 100×10^{-3} M) was dropwise added to initialize the micellization, followed by a dialysis to remove the organic solvent, as described in detail before.[27]

Diameter, size distribution, and zeta potentials of the micelles and both staphylococcal strains were measured at 25 °C using a Zetasizer Nano-ZS (Malvern Instruments, Worcestershire, UK) in 10×10^{-3} M potassium phosphate buffer at pH 5.0 and 7.4. The micelle concentration was 0.5 mg mL^{-1}, while bacteria were suspended to a concentration 1×10^{8} bacteria mL^{-1}. SSPMs or MSPMs were also characterized after exposure to plasma at pH 7.4. To this end, a micelle suspension (0.2 mg mL^{-1}) was mixed with 10% murine plasma (Sigma-Aldrich) in 10×10^{-3} M phosphate buffer at pH 7.4 for 24 h at 37 °C after which the suspension was filtrated using ultrafiltration centrifuge (filter cut-off size: 0.2 μm, 10 000 *g*, 5 min) to separate the micelles from

unadsorbed plasma proteins and micelles were resuspended in buffer for measurements.

ROS Generation Efficiency. In order to determine the ROS generation efficiency a water-soluble ROS trap ADA was used. Briefly, freshly prepared PpIX-loaded SSPMs or MSPMs (0.2 mg mL^{-1}) was mixed with ADA solution (10×10^{-6} M) and added to a cuvette. The cuvettes were irradiated with a LED light source (wavelength: 630 ± 30 nm, power density: 20 mW cm^{-2}). The UV–VIS absorption spectrum variations were recorded on an UV-2550 UV–VIS spectrophotometer (Shimadzu, Kyoto, Japan) every minute up to 10 min. The ROS trapping by ADA was monitored via decreasing of ADA UV–VIS absorption at 380 nm and 401 nm.

Bacterial Culturing and Harvesting. Two multidrug-resistant staphylococcal strains were employed in this study: green-fluorescent *S. aureus* WH^{GFP} and commercially available bioluminescent *S. aureus* Xen36 (PerkinElmer Inc., Waltham, MA, USA). Bioluminescent *S. aureus* Xen36 originates from *S. aureus* ATCC49525, a clinical strain isolated from bacteremia patient and made bioluminescent by inserting a modified Photorhabdus luminescens *lux*ABCDE operon into the bacterial genome.[62] Its bioluminescence requires adenosine tri-phosphate (ATP) and nicotinamide adenine dinucleotide phosphate hydrogen (NADPH) to maintain a sufficiently high level of aldehydes for the emission of light (see Figure **S4**, Supporting Information). Both strains were cultured at 37 °C in ambient air. *S. aureus* WH^{GFP} was cultured on agar plates with 10 μg mL^{-1} tetracycline, while *S. aureus* Xen36 was cultured on agar plates with 200 μg mL^{-1} kanamycin. For experiments, bacteria were cultured and harvested according to our previous protocol[27] and suspended in (PBS, 5×10^{-3} M K_2HPO_4, 5×10^{-3} M KH_2PO_4, and 150×10^{-3} M NaCl, pH 7.0) to concentrations required in the respective experiments, as determined in a Bürker–Türk counting chamber. pH of the suspension was adjusted when the experiment required so, through titration of aqueous solutions of diluted hydrochloric acid or potassium hydroxide.

Micelle Interactions with Mammalian Cells versus Staphylococci. First, mammalian cells were cultured, HUVEC were isolated from fresh umbilical cords after treatment with collagenase. HSF were kindly provided by Dr. Theo van Kooten (Universitair Medisch Centrum Groningen, The Netherlands), while Caco-2 were purchased from Sigma-Aldrich (ATCC CRL-2102). HUVEC and HSF were cultured in RPMI 1640 media supplemented with 0.1% GlutaMAX-I, 0.1% GA-1000 (gentamicin, amphotericin-B), and 20% fetal bovine serum for HUVEC and 10% for HSF. Caco-2 were grown in Dulbecco's modified Eagle medium with 20% fetal calf serum and 1% nonessential amino acids.

To demonstrate preferential interaction of the micelles with staphylococci over mammalian cells, mammalian cells (10^5 cells mL^{-1}) were seeded into 6 well plates (3×10^5 cells per well), and cultured at 37 °C for 24 h. After removal of the growth medium, *S. aureus* WH^{GFP} (10^8 bacteria mL^{-1}) were jointly suspended in 10×10^{-3} M phosphate buffer and freshly prepared Nile red-loaded MSMPs were added to each well with pH adjusted to pH 5.0 or pH 7.4. Interaction was allowed for 60 min at 37 °C, after which the suspension was removed and rinsed with PBS (1 mL $well^{-1}$). The cells were fixed with 3.7% paraformaldehyde solution for 15 min at ambient temperature and permeabilized with 0.1% Triton X-100 (1 mL $well^{-1}$) in PBS. Nuclei were stained with 4′,6-diamidino-2-phenylindole (DAPI) solution in PBS (4 μg mL^{-1}) for 1 h at room temperature. Cells were observed using a confocal laser scanning microscopy (TCS SP2, Leica, Wetzlar, Germany), equipped with an argon ion laser at 488 nm to excite Nile red and a violet (405 nm) laser to excite DAPI. Fluorescence was detected at 430–500 nm (blue) and 583–688 nm (red), respectively.

Killing of Planktonic Staphylococci by PpIX-Loaded Micelles. In order to determine staphylococcal killing by PpIX-loaded micelles, 100 μL of a staphylococcal suspension in PBS at pH 7.4 was mixed with 100 μL of each micelle suspension with a micelle concentration range of 0–160 μg mL^{-1}. After different light-activation times at 630 ± 30 nm using a 12× 8 LED matrix with a power density of 20 mW cm^{-2}, aliquots were taken from the suspensions and serially diluted. 10 μL diluted suspension was spread

over a TSB agar plate and incubated for 24 h at 37 °C after which the number of CFUs were counted. For controls, buffer and unloaded micelles (80 μg mL^{-1}) were used, as well as PpIX-loaded micelles in absence of light-activation. The experiments were done in triplicate with separately grown bacterial cultures. In similar experiments, staphylococcal killing in suspension as a function of light-activation time was evaluated from the bioluminescence of the suspensions using a bio-optical imaging system (IVIS Lumina II Imaging System, Perkin Elmer). Bioluminescence images (image acquisition factors: 20 s exposure time, medium binning, 1 F/Stop, Open Emission Filter) were taken every 5 min light-activation. Light-activation was applied for 5 min periods with 10 min intervals in between up to a total of 20 min lightactivation time. Images were automatically corrected for background noise. Regions of interest (ROIs) were manually created for each well and average radiances over the ROIs were converted to photon fluxes (p/s) using Living Image software (Perkin Elmer).

Killing of Staphylococci in Their Biofilm Mode of Growth by PpIX Loaded Micelles. In order to determine the killing efficiency of staphylococci in their biofilm mode of growth by PpIX-loaded micelles, biofilms were grown by adding 100 μL of staphylococcal suspension (10^8 bacteria mL^{-1}) in PBS to 96-wells plates at 37 °C for 1 h to allow bacteria to adhere. Next, bacterial suspensions were removed and the wells were washed with 100 μL PBS. Subsequently, 200 μL TSB was added and adhering bacteria were grown into a biofilm for 48 h at 37 °C. Then, TSB medium was replaced by 100 μL of PpIX-loaded SSPMs or MSPMs (0–160 μg mL^{-1}) in PBS for 2 h. After 2 h incubation at 37 °C, micelle suspension was removed from wells and the biofilms were rinsed with 100 μL PBS. Light-activation was applied for 5 min periods with 10 min intervals in between up to 40 min total lightactivation time. After each light-activation, biofilms were scraped off a well and staphylococci suspended in PBS pH 7.4 and serially diluted up to 10^6 fold. 10 μL of each diluted was spread over a TSB agar plate for 24 h incubation at 37 °C and the CFUs were counted. In a separate experiment, biofilms were imaged immediately after each lightactivation, as described above.

Murine Skin Infection Model. BALB/c nude mice (18–20 g each) were obtained from Vital River Laboratory Animal Technology Co. (Beijing, China). All animals were housed in the on-site animal facility of Nankai University and experimental procedures were approved by the Institutional Animal Care and Use Committee of Nankai University, Tianjin, China. Two subcutaneous infection sites were created in each mouse by injecting a dose of 2×10^7 bioluminescent and vancomycinresistant (see also Table **S1**, Supporting Information) *S. aureus* Xen36 in the left and right flanks of the mice to initiate infection. Bioluminescent intensity and area were recorded using a bio-optical imaging system (IVIS, 45 s exposure time, medium binning, 1 F/Stop, Open Emission Filter). Images were analyzed using "Image J" (NIH Research Services Branch, USA) software.[63]

Since bioluminescence reached a maximum at day 2 after injection (Figure **S3**, Supporting Information), infected animals were randomly assigned after two days into four groups of six animals each, receiving either daily, subcutaneous injection (i) 154×10^{-3} M saline (untreated control), (ii) 200 μL vancomycin in PBS (10 mg mL^{-1} yielding 120 mg vancomycin per kg body weight), (iii) 100 μL SSPM + PpIX (5 mg mL^{-1}, light-activated for 30 min at 1 h postinjection), and (iv) 100 μL MSPM + PpIX (5 mg mL^{-1}, light-activated for 30 min at 1 h postinjection). Antibiotic regimen was designed to achieve a concentration above the minimal inhibitory concentration (MIC) of susceptible strains in serum, based on the use of a similar murine model in the literature.[64] Treatment was initiated 2 d postinfection and continued for 5 consecutive days. Bioluminescent imaging was performed daily, after daily light activation.

In order to follow the trajectory of injected micelles, MSPMs were loaded with fluorescent Cy5.5, as described above for Nile red-loading, mixing Cy5.5-PEG-b-PCL (2 mg, 10 wt% with respect to the total amount of polymer) with PEG-*b*-PCL (8 mg mL^{-1}) and PCL-*b*-PAE (10 mg mL^{-1}) in dimethylformamide to a total volume of 4 mL (Figure **S5**, Supporting Information). Subsequently 15 BALB/c nude mice were intravenously injected with 200 μL Cy5.5-labeled MSPMs (5 mg mL^{-1}) and divided into 5 groups of 3 mice

each. At different points in time after injection up to 48 h, mice in one group were sacrificed and heart, liver, spleen, lungs, and kidneys surgically removed of fluorescent examination on a IVIS Lumina XR system as described above at an excitation wavelength of 640 nm and emission at 694 nm. Also after injection till sacrifice in the 48 h group**,** urine was collected at the different time points and its fluorescence measured.

Statistical Analysis. All data were expressed as means ± SD values. Differences between groups were examined for statistical significance with two-tailed Student's *t*-test. Differences were considered significance at $p < 0.05$.

REFERENCES

(1) Hall-Stoodley, L.; Costerton, J. W.; Stoodley, P. Bacterial Biofilms: from the Natural Environment to Infectious Diseases. *Nat. Rev. Microbiol.* **2004**, *2*, 95–108.

(2) Flemming, H.-C.; Wingender, J. The Biofilm Matrix. *Nat. Rev. Microbiol.* **2010**, *8*, 623–633.

(3) Costerton, J. W.; Stewart, P. S.; Greenberg, E. P. Bacterial Biofilms: A Common Cause of Persistent Infections. *Science* **1999**, *284*, 1318–1322.

(4) Stewart, P. S.; Costerton, J. W. Antibiotic Resistance of Bacteria in Biofilms. *Lancet* **2001**, *358*, 135–138.

(5) Flemming, H.-C.; Wingender, J.; Szewzyk, U.; Steinberg, P.; Rice, S. A.; Kjelleberg, S. Biofilms: An Emergent Form of Bacterial Life. *Nat. Rev. Microbiol.* **2016**, *14*, 563–575.

(6) Levy, S. B.; Marshall, B. Antibacterial Resistance Worldwide: Causes, Challenges and Responses. *Nat. Med.* **2004**, *10*, S122–S129.

(7) Gordon, J. I.; Klaenhammer, T. R. A Rendezvous with Our Microbes. *Proc. Natl. Acad. Sci. U. S. A.* **2011**, *108*, 4513–4515.

(8) Davies, D. Understanding Biofilm Resistance to Antibacterial Agents. *Nat. Rev. Drug Discovery* **2003**, *2*, 114–122.

(9) Baym, M.; Stone, L. K.; Kishony, R. Multidrug Evolutionary Strategies to Reverse Antibiotic Resistance. *Science* **2016**, *351*, aad3292.

(10) Riool, M.; de Breij, A.; de Boer, L.; Kwakman, P. H.; Cordfunke, R. A.; Cohen, O.; Malanovic, N.; Emanuel, N.; Lohner, K.; Drijfhout, J. W. Controlled Release of LL-37-Derived Synthetic Antimicrobial and Anti-Biofilm Peptides SAAP-145 and SAAP-276 Prevents Experimental Biomaterial-Associated *Staphylococcus aureus* Infection. *Adv. Funct. Mater.* **2017**, *27*, 1606623.

(11) Brown, D. Antibiotic Resistance Breakers: Can Repurposed Drugs Fill the Antibiotic Discovery Void? *Nat. Rev. Drug Discovery* **2015**, *14*, 821.

(12) Brown, E. D.; Wright, G. D. Antibacterial Drug Discovery in the Resistance Era. *Nature* **2016**, *529*, 336.

(13) Dolmans, D. E.; Fukumura, D.; Jain, R. K. Photodynamic Therapy for Cancer. *Nat. Rev. Cancer* **2003**, *3*, 380.

(14) Castano, A. P.; Mroz, P.; Hamblin, M. R. Photodynamic Therapy and Anti-Tumour Immunity. *Nat. Rev. Cancer* **2006**, *6*, 535.

(15) Spring, B. Q.; Sears, R. B.; Zheng, L. Z.; Mai, Z.; Watanabe, R.; Sherwood, M. E.; Schoenfeld, D. A.; Pogue, B. W.; Pereira, S. P.; Villa, E. A Photoactivable Multi-Inhibitor Nanoliposome for Tumour Control and Simultaneous Inhibition of Treatment Escape Pathways. *Nat. Nanotechnol.* **2016**, *11*, 378.

(16) Idris, N. M.; Gnanasammandhan, M. K.; Zhang, J.; Ho, P. C.; Mahendran, R.; Zhang, Y. *In Vivo* Photodynamic Therapy Using Upconversion Nanoparticles as Remote-Controlled Nanotransducers. *Nat. Med.* **2012**, *18*, 1580.

(17) Chen, W. Y.; Chang, H. Y.; Lu, J. K.; Huang, Y. C.; Harroun, S. G.; Tseng, Y. T.; Li, Y. J.; Huang, C. C.; Chang, H. T. Self-Assembly of Antimicrobial Peptides on Gold Nanodots: Against Multidrug-Resistant Bacteria and Wound-Healing Application. *Adv. Funct. Mater.* **2015**, *25*, 7189–7199.

(18) Courtney, C. M.; Goodman, S. M.; McDaniel, J. A.; Madinger, N. E.; Chatterjee, A.; Nagpal, P. Photoexcited Quantum Dots for Killing Multidrug-Resistant Bacteria. *Nat. Mater.* **2016**, *15*, 529.

(19) Xing, C.; Xu, Q.; Tang, H.; Liu, L.; Wang, S. Conjugated Polymer/Porphyrin Complexes for Efficient Energy Transfer and Improving Light-Activated Antibacterial Activity. *J. Am. Chem. Soc.* **2009**, *131*, 13117–13124.

(20) Zhu, C.; Yang, Q.; Liu, L.; Lv, F.; Li, S.; Yang, G.; Wang, S. Multifunctional Cationic Poly(p-phenylene vinylene) Polyelectrolytes for Selective Recognition, Imaging, and Killing of Bacteria Over Mammalian Cells. *Adv. Mater.* **2011**, *23*, 4805–4810.

(21) Liu, C.; Kong, D.; Hsu, P.-C.; Yuan, H.; Lee, H.-W.; Liu, Y.; Wang, H.; Wang, S.; Yan, K.; Lin, D. Rapid Water Disinfection Using Vertically Aligned MoS_2 Nanofilms and Visible Light. *Nat. Nanotechnol.* **2016**, *11*, 1098.

(22) Zanin, I. C. J.; Goncalves, R. B.; Junior, A. B.; Hope, C. K.; Pratten, J. Susceptibility of *Streptococcus mutans* Biofilms to Photodynamic Therapy: An *In Vitro* Study. *J. Antimicrob. Chemother.* **2005**, *56*, 324–330.

(23) Kim, S.; Ohulchanskyy, T. Y.; Pudavar, H. E.; Pandey, R. K.; Prasad, P. N. Organically Modified Silica Nanoparticles Co-Encapsulating Photosensitizing Drug and Aggregation-Enhanced Two-Photon Absorbing Fluorescent Dye Aggregates for Two-Photon Photodynamic Therapy. *J. Am. Chem. Soc.* **2007**, *129*, 2669–2675.

(24) Lucky, S. S.; Soo, K. C.; Zhang, Y. Nanoparticles in Photodynamic Therapy. *Chem. Rev.* **2015**, *115*, 1990–2042.

(25) Zhang, Z.; Ma, R.; Shi, L. Cooperative Macromolecular Self-Assembly toward Polymeric Assemblies with Multiple and Bioactive Functions. *Acc. Chem. Res.* **2014**, *47*, 1426–1437.

(26) Huang, F.; Wang, J.; Qu, A.; Shen, L.; Liu, J.; Liu, J.; Zhang, Z.; An, Y.; Shi, L. Maintenance of Amyloid β Peptide Homeostasis by Artificial Chaperones Based On Mixed-Shell Polymeric micelles. *Angew. Chem., Int. Ed.* **2014**, *53*, 8985–8990.

(27) Liu, Y.; Busscher, H. J.; Zhao, B.; Li, Y.; Zhang, Z.; Van Der Mei, H. C.; Ren, Y.; Shi, L. Surface-Adaptive, Antimicrobially Loaded, Micellar Nanocarriers with Enhanced Penetration and Killing Efficiency in Staphylococcal Biofilms. *ACS Nano* **2016**, *10*, 4779–4789.

(28) Vroom, J. M.; De Grauw, K. J.; Gerritsen, H. C.; Bradshaw, D. J.; Marsh, P. D.; Watson, G. K.; Birmingham, J. J.; Allison, C. Depth Penetration and Detection of pH Gradients in Biofilms by Two-Photon Excitation Microscopy. *Appl. Environ. Microbiol.* **1999**, *65*, 3502–3511.

(29) Simmen, H.-P.; Battaglia, H.; Giovanoli, P.; Blaser, J. Analysis of pH, pO_2 and pCO_2 in Drainage Fluid Allows for Rapid Detection of Infectious Complications During the Follow-up Period after Abdominal Surgery. *Infection* **1994**, *22*, 386–389.

(30) Radovic-Moreno, A. F.; Lu, T. K.; Puscasu, V. A.; Yoon, C. J.; Langer, R.; Farokhzad, O. C. Surface Charge-Switching Polymeric Nanoparticles for Bacterial Cell Wall-Targeted Delivery of Antibiotics. *ACS Nano* **2012**, *6*, 4279–4287.

(31) Chu, L.; Gao, H.; Cheng, T.; Zhang, Y.; Liu, J.; Huang, F.; Yang, C.; Shi, L.; Liu, J. A Charge-Adaptive Nanosystem for Prolonged and Enhanced: *In Vivo* Antibiotic Delivery. *Chem. Commun.* **2016**, *52*, 6265–6268.

(32) Yue, J.; Zhao, P.; Gerasimov, J. Y.; van de Lagemaat, M.; Grotenhuis, A.; Rustema-Abbing, M.; van der Mei, H. C.; Busscher, H. J.; Herrmann, A.; Ren, Y. 3D-Printable Antimicrobial Composite Resins. *Adv. Funct. Mater.* **2015**, *25*, 6756–6767.

(33)Thammavongsa, V.; Kim, H. K.; Missiakas, D.; Schneewind, O. Staphylococcal Manipulation of Host Immune Responses. *Nat. Rev. Microbiol.* **2015**, *13*, 529.

(34) Tenzer, S.; Docter, D.; Kuharev, J.; Musyanovych, A.; Fetz, V.; Hecht, R.; Schlenk, F.; Fischer, D.; Kiouptsi, K.; Reinhardt, C. Rapid Formation of Plasma Protein Corona Critically Affects Nanoparticle Pathophysiology. *Nat. Nanotechnol.* **2013**, *8*, 772.

(35) Monopoli, M. P.; Åberg, C.; Salvati, A.; Dawson, K. A. Biomolecular Coronas Provide the Biological Identity of Nanosized Materials. *Nat. Nanotechnol.* **2012**, *7*, 779.

(36) Schöttler, S.; Becker, G.; Winzen, S.; Steinbach, T.; Mohr, K.; Landfester, K.; Mailänder, V.; Wurm, F. R. Protein Adsorption is Required for Stealth Effect of Poly (Ethylene Glycol)-and Poly (Phosphoester)-Coated Nanocarriers. *Nat. Nanotechnol.* **2016**, *11*, 372.

(37) Gao, G. H.; Lee, J. W.; Nguyen, M. K.; Im, G. H.; Yang, J.; Heo, H.; Jeon, P.; Park, T. G.; Lee, J. H.; Lee, D. S. pH-Responsive Polymeric Micelle Based on PEG-Poly (*β*-Amino Ester)/(Amido Amine) as Intelligent Vehicle for Magnetic Resonance Imaging in Detection of Cerebral Ischemic Area. *J. Control. Release* **2011**, *155*, 11–17.

(38) Whelan, H. T.; Smits Jr, R. L.; Buchman, E. V.; Whelan, N. T.; Turner, S. G.; Margolis, D. A.; Cevenini, V.; Stinson, H.; Ignatius, R.; Martin, T. Effect of NASA Light-Emitting Diode Irradiation on Wound Healing. *J. Clin. Laser Med. Surg.* **2001**, *19*, 305–314.

(39) Daghighi, S.; Sjollema, J.; Harapanahalli, A.; Dijkstra, R. J.; van der Mei, H. C.; Busscher, H. J. Influence of Antibiotic Pressure on Bacterial Bioluminescence, with Emphasis on *Staphylococcus aureus*. *Int. J. Antimicrob. Agents* **2015**, *46*, 713–717.

(40) van Staden, A. D. P.; Heunis, T.; Smith, C.; Deane, S.; Dicks, L. M. Efficacy of Lantibiotic Treatment of *Staphylococcus aureus*-Induced Skin Infections, Monitored by *In Vivo* Bioluminescent Imaging. *Antimicrob. Agents Chemother.* **2016**, AAC. 02938–02915.

(41) Van Oosten, M.; Schäfer, T.; Gazendam, J. A.; Ohlsen, K.; Tsompanidou, E.; De Goffau, M. C.; Harmsen, H. J.; Crane, L. M.; Lim, E.; Francis, K. P. Real-Time *In Vivo* Imaging of Invasive-and Biomaterial-Associated Bacterial Infections Using Fluorescently Labelled Vancomycin. *Nat. Commun.* **2013**, *4*, 3584.

(42) Wang, B.; He, X.; Zhang, Z.; Zhao, Y.; Feng, W. Metabolism of Nanomaterials *In Vivo*: Blood Circulation and Organ Clearance. *Acc. Chem. Res.* **2012**, *46*, 761–769.

(43) Casanova, J.-L.; Abel, L. The Human Model: A Genetic Dissection of Immunity to Infection in Natural Conditions. *Nat. Rev. Immunol.* **2004**, *4*, nri1264.

(44) Dwyer, D. J.; Kohanski, M. A.; Collins, J. J. Role of Reactive Oxygen Species in Antibiotic Action and Resistance. *Curr. Opin. Microbiol.* **2009**, *12*, 482–489.

(45) Moan, J.; BERG, K. The Photodegradation of Porphyrins in Cells Can Be Used to Estimate the Lifetime of Singlet Oxygen. *Photochem. Photobiol.* **1991**, *53*, 549–553.

(46) Velema, W. A.; Van Der Berg, J. P.; Hansen, M. J.; Szymanski, W.; Driessen, A. J.; Feringa, B. L. Optical Control

of Antibacterial Activity. *Nat. Chem.* **2013**, *5*, 924.

(47) Bai, H.; Lv, F.; Liu, L.; Wang, S. Supramolecular Antibiotic Switches: A Potential Strategy for Combating Drug Resistance. *Chem.–Eur. J.* **2016**, *22*, 11114–11121.

(48) Hamblin, M. R. Antimicrobial Photodynamic Inactivation: A Bright New Technique to Kill Resistant Microbes. *Curr. Opin. Microbiol.* **2016**, *33*, 67–73.

(49) Xiao, J.; Chen, S.; Yi, J.; Zhang, H. F.; Ameer, G. A. A Cooperative Copper Metal–Organic Framework-Hydrogel System Improves Wound Healing in Diabetes. *Adv. Funct. Mater.* **2017**, *27*, 1604872.

(50) Neut, D.; Tijdens-Creusen, E. J.; Bulstra, S. K.; van der Mei, H. C.; Busscher, H. J. Biofilms in Chronic Diabetic Foot Ulcers—A Study of 2 Cases. *Acta Orthop.* **2011**, *82*, 383–385.

(51) Brancaleon, L.; Moseley, H. Laser and Non-Laser Light Sources for Photodynamic Therapy. *Lasers Med. Sci.* **2002**, *17*, 173–186.

(52) Lovell, J. F.; Liu, T. W.; Chen, J.; Zheng, G. Activatable Photosensitizers for Imaging and Therapy. *Chem. Rev.* **2010**, *110*, 2839–2857.

(53) van Straten, D.; Mashayekhi, V.; de Bruijn, H. S.; Oliveira, S.; Robinson, D. J. Oncologic Photodynamic Therapy: Basic Principles, Current Clinical Status and Future Directions. *Cancers* **2017**, *9*, 19.

(54) Gaucher, G.; Dufresne, M.-H.; Sant, V. P.; Kang, N.; Maysinger, D.; Leroux, J.-C. Block Copolymer Micelles: Preparation, Characterization and Application in Drug Delivery. *J. Control. Release* **2005**, *109*, 169–188.

(55) Sun, Q.; Radosz, M.; Shen, Y. Challenges in Design of Translational Nanocarriers. *J. Control. Release* **2012**, *164*, 156–169.

(56) Lynn, D. M.; Langer, R. Degradable Poly (β-Amino Esters): Synthesis, Characterization, and Self-Assembly with Plasmid DNA. *J. Am. Chem. Soc.* **2000**, *122*, 10761–10768.

(57) Agostinis, P.; Berg, K.; Cengel, K. A.; Foster, T. H.; Girotti, A. W.; Gollnick, S. O.; Hahn, S. M.; Hamblin, M. R.; Juzeniene, A.; Kessel, D. Photodynamic Therapy of Cancer: An Update. *CA. Cancer J. Clin.* **2011**, *61*, 250–281.

(58) Busscher, H. J.; Van Der Mei, H. C.; Subbiahdoss, G.; Jutte, P. C.; Van Den Dungen, J. J.; Zaat, S. A.; Schultz, M. J.; Grainger, D. W. Biomaterial-Associated Infection: Locating the Finish Line in the Race for the Surface. *Sci. Transl. Med.* **2012**, 4, 153rv110.

(59) Darouiche, R. O. Antimicrobial Approaches for Preventing Infections Associated with Surgical Implants. *Clin. Infect. Dis.* **2003**, *36*, 1284–1289.

(60) Grainger, D. W.; van der Mei, H. C.; Jutte, P. C.; van den Dungen, J. J.; Schultz, M. J.; van der Laan, B. F.; Zaat, S. A.; Busscher, H. J. Critical Factors in the Translation of Improved Antimicrobial Strategies for Medical Implants and Devices. *Biomaterials* **2013**, *34*, 9237–9243.

(61) Moriarty, T.; Grainger, D.; Richards, R. Challenges in Linking Preclinical Anti-Microbial Research Strategies with Clinical Outcomes for Device-Associated Infections. *Eur. Cell. Mater.* **2014**, *28*, 112–128.

(62) Hastings, J. W.; Nealson, K. H. Bacterial Bioluminescence. *Annu. Rev. Microbiol.* **1977**, *31*, 549–595.

(63) Schindelin, J.; Arganda-Carreras, I.; Frise, E.; Kaynig, V.; Longair, M.; Pietzsch, T.; Preibisch, S.; Rueden, C.; Saalfeld, S.; Schmid, B. Fiji: An Open-Source Platform for Biological-Image Analysis. *Nat. Meth.* **2012**, *9*, 676.

(64) Crandon, J. L.; Kuti, J. L.; Nicolau, D. P. Comparative Efficacies of Human Simulated Exposures of Telavancin and Vancomycin against Methicillin-Resistant *Staphylococcus aureus* with a Range of Vancomycin MICs in a Murine Pneumonia Model. *Antimicrob. Agents Chemother.* **2010**, *54*, 5115–5119.

SUPPORTING INFORMATION

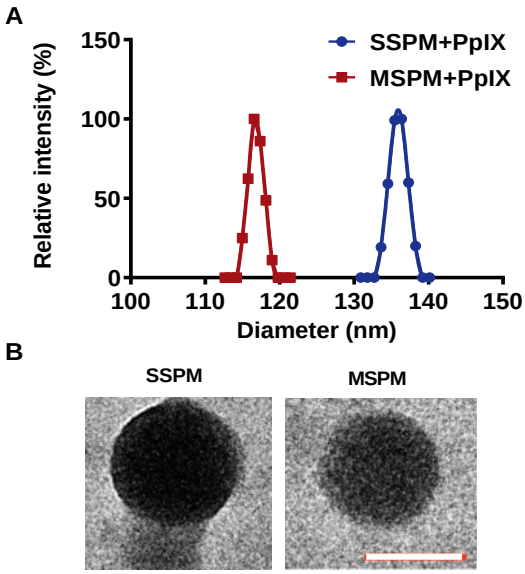

Figure S1. Micelle morphology. (**A**) Micelle diameters distribution of PpIX-loaded MSPMs and SSPMs at pH 7.4, measured using dynamic light scattering. (**B**) Transmission electron micrographs of PpIX-loaded SSPM and MSPMs. Scale bar indicates 100 nm for both images.

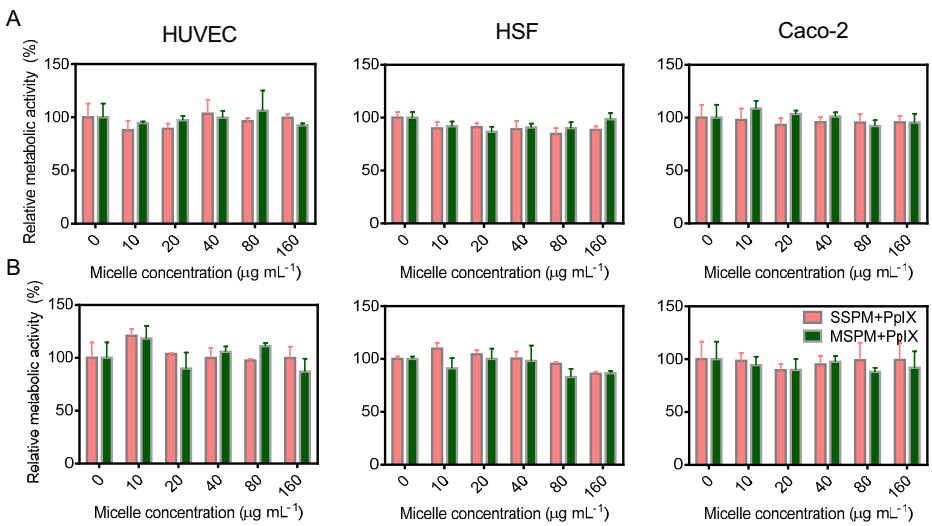

Figure S2. Biocompatibility of mammalian cells with PpIX-loaded SSPMs and MSPMs and their light-activated ROS generation. (**A**) Relative metabolic activity of HUVEC, HSF and Caco-2 cells after 24 h growth in the presence of PpIX-loaded SSPMs and MSPMs as a function of the micelle concentration. Metabolic activity in absence of micelles was set at 100%. (**B**) Same as panel (a), now after 15 min light-activation at the onset of growth. Metabolic activity in

absence of micelles was set at 100%. All data are expressed as means ± SD values over triplicate experiments with separately prepared micelles and different cell cultures. Metabolic activity was quantitated using an MTT assay. Cells (5×10^4 cell mL^{-1}) were seeded in gelatin-coated 96-well plates and incubated at 37°C and 5% CO_2 for 24 h, after which the supernatant was removed, 100 μL micelle suspension with different concentrations of micelles added (0–160 μg mL^{-1}) in growth medium was added to each well for 24 h incubation at 37°C. Subsequently, growth medium was replaced by 100 μL MTT (Sigma-Aldrich, 1 mg mL^{-1}) in growth medium. After 4 h, supernatant was removed and 100 μL i-propanol was added to dissolve violet crystals and absorbance was measured at 560 nm on a Fluostar® microplate reader (Ortenberg, Germany). Experiments were carried out with and without light-activation (15 min) of the PpIX-loaded micelles.

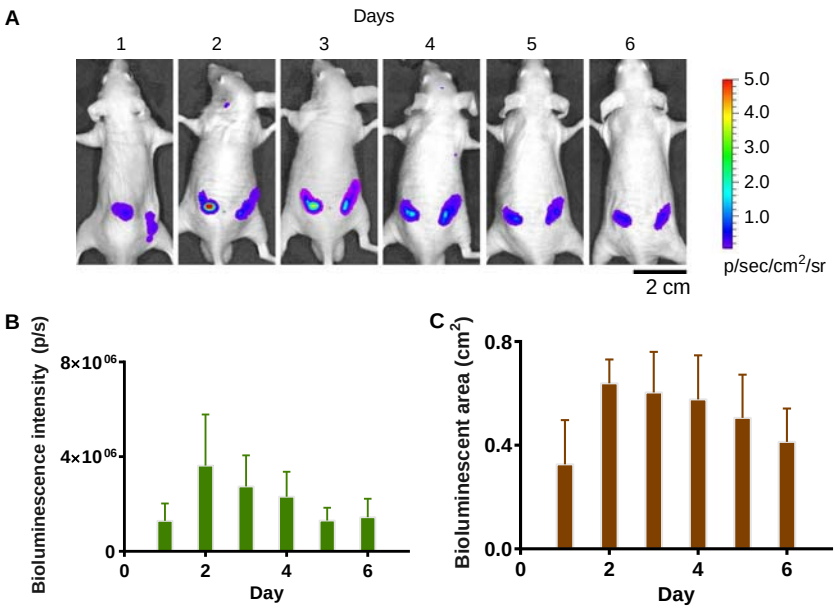

Figure S3. Development of bioluminescence of a sub-cutaneous, vancomycin-resistant staphylococcal infection in a murine model without treatment, studied using bio-optical imaging. Mice were sub-cutaneously injected at t = 0 at two sites with a suspension of bioluminescent *S. aureus* Xen36 (20 μL, 10^9 bacteria mL^{-1}). (**A**) Time series of bioluminescence images for one and the same mouse after injection of a staphylococcal suspension in absence of treatment. (**B**) Bioluminescence flux as a function of time after staphylococcal injection, averaged over left and right injection sites in six animals. Error bars indicate SD values over six animals. (**C**) Same as panel B, now for the bioluminescent area of the infected site.

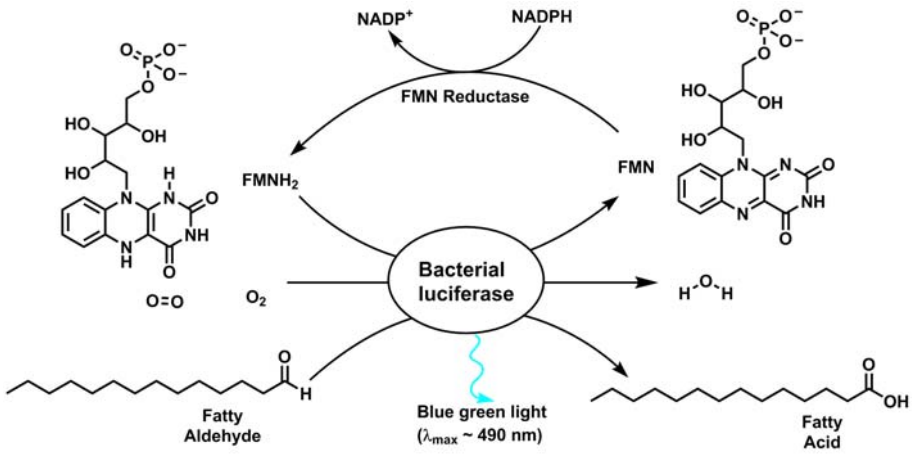

Figure S4. Biochemical mechanisms of bacterial bioluminescence production.[62]

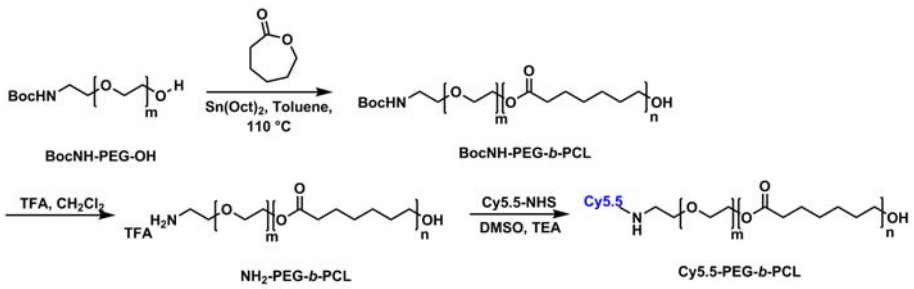

Figure S5. Synthesis route of Cy5.5-poly(ethylene glycol)-*block*-poly(ε-caprolactone) (Cy5.5-PEG-*b*-PCL). Boc refers to t-butyloxy carbonyl group, TFA to trifluoroacetic acid, Cy5.5-NHS (95%, Sigma-Aldrich) to Cy5.5 mono N-hydroxysuccinamide ester, DMSO to dimethyl sulphoxide, and TEA to trimethylamine.

NOTES